THREE-DIMENSIONAL MAPPING OF LIGHT TRANSMITTANCE AND FOLIAGE DISTRIBUTION USING LIDAR

Kenton Todd[1], Ferenc Csillag*[1], and Peter Atkinson[2]

*Corresponding author

[1] Department of Geography and Institute for Land Information Management, University of Toronto, Mississauga, Ontario, Canada L5L 1C6 (fcs@geog.utoronto.ca)

[2] Department of Geography, University of Southampton, Highfield, Southampton, United Kingdom SO17 1BJ (P.M.Atkinson@soton.ac.uk)

ABSTRACT

The horizontal and vertical distribution of light transmittance was evaluated as a function of foliage distribution using LiDAR (Light Detection and Ranging) observations for a sugar maple (*Acer Saccharum*) stand in the Turkey Lakes Watershed. Along the vertical profile of vegetation horizontal slices of probability of light transmittance were derived from an Optech ALTM 1225 instrument's return pulses (two discrete, 15 cm diameter returns) using indicator kriging. These predictions were compared with (1) below canopy (1 cm spatial resolution) transect measurements of photosynthetically-active radiation (PAR) using hand-held quantum sensors and (2) a traditional forest inventory of tree height. Local minimum and maximum filters were applied to the raw ground and vegetation returns to reduce bias and a first-order trend was removed to ensure stationarity. The vertical distribution of vegetation height was sliced into ten percentiles and indicator variograms were fitted to them. Variogram parameters varied as a function of foliage thickness and height above ground. Ground measurements of PAR showed high correlation with kriged light transmittance probabilities and this relationship becomes tighter with coarser spatial resolution. Three-dimensional maps of foliage distribution were computed as stacks of the percentile probability surfaces (*i.e.*, probability of a LiDAR pulse being returned from foliage at a given height within the canopy). These probability surfaces showed good correspondence with individual tree-based observations and provide a much more detailed characterization of quasi-continuous foliage distribution. These results suggest that discrete-return LiDAR provides a promising technology to capture variations of foliage characteristics in forests, providing functional linkages between biophysical and ecological studies.

KEYWORDS

LiDAR, PAR, forest structure, vegetation height, indicator kriging

INTRODUCTION

As part of recent sustainable forestry initiatives in Canada, forest ecosystem models are required to evaluate spatial and temporal changes in both forest structure and carbon and nitrogen cycling. Several research programs have focused on implementing policy (IPCC, 2001) and alternative forestry practices (CCFM, 1997) to enhance biomass production and reduce atmospheric carbon. Forest biophysical variables, such as leaf area index (LAI) and net primary productivity (NPP), are used directly to monitor changes in carbon and nitrogen within forest environments. LAI has been found to control levels of carbon dioxide, water and energy exchanged between the biosphere and atmosphere (Waring and Running, 1998). NPP provides a measure of the amount of carbon absorption by plants, allowing carbon sinks to be identified. Predictions of LAI and NPP have been created recently for international (Goodale *et al*., 2002) and national extents (Chen *et al*., 1999; Chen *et al*., 2000). While coarse spatial resolution predictions of NPP and LAI are traditionally validated using stand-level clippings of vegetation, more detailed information on vegetation volume and structure would facilitate greater accuracy assessment (Lieth and Whittaker, 1975; Chen *et al*., 1999).

The provision of fine resolution remotely-sensed information on forest structure is made difficult by several factors. The three-dimensional characteristics of forest canopy environments prevent optical remote sensing instruments from providing structural information in areas of dense vegetation cover (Chen, 1996). Further, the majority of remote sensing instruments operate at spatial resolutions that are too coarse to capture individual forest structural components. Fine spatial resolution remote sensing data are required that can be aggregated spatially to produce a spatial resolution sensitive to the forest attributes under investigation (Treitz and Howarth, 1996; Treitz, 2001).

Knowledge on the three-dimensional light regime within forest canopies is requisite for accurate predictions of both LAI and NPP and evaluation of forest stand development. For example, Farquhar's photosynthesis model requires information on sunlit and shaded leaf groups or on the layering of canopy

vegetation to provide greater accuracy in predictions of regional plant growth and the carbon budget (Chen *et al*., 1999). Many factors influence the dynamics of light within a forest canopy environment. The horizontal and vertical distribution of light and foliage occur in a complementary fashion, with light transmittance being dependent on the presence, size and arrangement of canopy gaps (Parker, 1995). Currently, several hand-held optical instruments are available for determining light transmittance. However, several constraints restrict the sampling process: (*i*) temporal implications of solar angle and atmospheric interference, (*ii*) lack of access to measurements along the entire vertical forest profile, and (*iii*) lack of high density observations over larger forested areas.

Forest growth and yield have traditionally been monitored using allometric measurements of forest structure (*e.g*., diameter at breast height (DBH), tree height and tree volume). Allometric measurements provide a valuable description of forest structure with the limitation that observations are often available only for harvested areas and developed from volume tables and standardized equations. While traditional allometric measurements can be used to quantify forest structure for individual trees, plots or stands (with spatial resolution ranging from square metres to hectares), ground observations for larger forested landscapes are not feasible due to the density of samples required. Future directions for monitoring forest growth and yield will require more detailed samples of vegetation structure to address local changes occurring by species, age and site condition.

LiDAR (Light Detection And Ranging) remote sensing has generated great interest recently because of its potential to provide forest biophysical variables with greater spatial detail and accuracy. LiDAR is an active remote sensing instrument operating similarly to a laser ranger by obtaining multiple measurements of distance and energy on a path between the laser instrument and a reflective surface. Vertical height measurements of forest canopy and ground surfaces can be obtained by setting appropriately the reflection threshold values for the laser return pulse.

Two types of LiDAR devices are currently in use: (*i*) small-footprint, discrete-return LiDAR, and (*ii*) large-footprint, full-waveform LiDAR. Large-footprint, full-waveform LiDAR instruments operate with a footprint diameter of = 10 m ground area. An associated reflectance waveform is created for each footprint to monitor changes in the characteristics of the reflectance surface. Large-footprint, full-waveform LiDAR has been used recently to accurately predict forest biophysical variables (Lefsky, 1997; Lefsky *et al.*, 1999a; Lefsky *et al.*, 1999b; Means *et al.*, 1999). A study by Parker *et al.* (2001) recently explored the association between light transmittance in forest canopies and the digitized waveform return from large-footprint, full-waveform LiDAR. The spatial variation in light transmittance was found to vary as a function of canopy height and could be replicated using digitized waveform data. However, large-footprint, full-waveform LiDAR is used exclusively for research purposes due to provision costs and data storage limitations (Flood, 2002).

The density of three-dimensional measurements provided by small-footprint, discrete-return LiDAR may facilitate accurate prediction of forest structural variables for several reasons. First, with footprint return densities of up to 2 – 3 returns/m^2 and footprint diameters of 15 cm, detailed structural components of a forest canopy (*e.g.*, gaps, crown edges, and inner-crown vegetation) may be captured. Second, due to this high density of laser returns, observations can be spatially aggregated to correspond with the spatial character of the forest environment.

Alternative methods of deriving forest structural variables must also be explored with respect to the characteristics of small-footprint, discrete-return LiDAR. Since LiDAR vegetation-returns are not located continuously along the vertical profile of a forest canopy (Lim *et al.*, 2001) an extreme range of height measurements will occur over short spatial distances. Further, Harding (2002) suggests that although discrete-return systems achieve a high density of spatial observations, the ground and vegetation returns suffer from leading-edge ranging bias, where the peak in the backscatter return energy is not measured consistently for the leading-edge return due to differences in vegetation structure (Harding *et al.*, 2001).

116 The ability to obtain a return from the outer canopy surface is dependent on the geometry, degree of
117 clumping and the reflective characteristics of the foliage. The implication is that direct interpolation of
118 the LiDAR discrete-return information will not provide an accurate prediction of the canopy surface or
119 the internal canopy structure due to this bias. However, spatial filtering techniques may be used to
120 remove this bias.
121
122 The goal of this research was to obtain spatially explicit vertical and horizontal distributions of
123 foliage and light transmittance. Two main objectives were proposed to achieve this goal: (*i*) to identify an
124 interpolation and mapping technique for developing three-dimensional models of forest structure from
125 LiDAR data and (*ii*) to determine the accuracy of the interpolation technique using ground measures of
126 forest structure. Two specific ground measures of forest structure were selected to assess the accuracy of
127 the interpolated surfaces from LiDAR: (*i*) the distribution of canopy gaps (open space) obtained from
128 light transmittance measurements and (*ii*) maximum tree height measured on a per-stem basis. A
129 systematic approach was taken based on the characteristics of the LiDAR data. First, we used a filtering
130 technique to limit the effects of the ranging bias from the leading-edge return pulses. Global trends in the
131 ground observations were removed, after which ordinary kriging was used to interpolate the digital
132 elevation model (DEM). Next, vegetation height was determined from vegetation first-return pulses by
133 subtracting the interpolated ground elevation from each vegetation first-return pulse. Vegetation
134 probability surfaces were then interpolated using indicator kriging for a series of thresholds defined using
135 the nine percentiles of vegetation height. Each threshold surface provides a continuous measure of
136 vegetation probability (*i.e.*, the probability of a LiDAR pulse being returned from foliage at the associated
137 threshold height). Finally, we assessed the accuracy of the predicted vegetation probability surfaces using
138 ground-based observations of tree height and light transmittance.
139
140

METHODS

Study Site

The study site for this paper is the Turkey Lakes Watershed (TLW), located in the Algoma District of northern Ontario, Canada, approximately 60 km north of the city of Sault Ste. Marie and 13 km inland from Lake Superior's shoreline. Since 1997, the Canadian Forest Service has been conducting the Turkey Lakes Harvesting Impacts Project (TLHIP) in the watershed. Variation in silvicultural practices are monitored within several harvest blocks where single-tree selection, shelterwood, and clear-cut harvesting has been performed (see Morrison *et al*. 1999). The focus of this study is a one hectare shelterwood site where shelterwood cutting was performed in 1997 (**Figure 1**). Shelterwood cutting is the practice of removing lower-strata trees to allow regeneration of lower vegetation for future harvesting purposes (Oliver, 1990). The site is occupied by 733 trees that are primarily remnant, uneven-aged sugar maple (*Acer saccharum*, 88 %) and yellow birch (*Betula alleghaniensis*, 6 %) with smaller percentages of iron wood (*Ostrya Virginiana*, 4 %), white birch (*Betula papyrifera*, 1 %) and white spruce (*Picea glauca*, 1 %). Evidence of shelterwood harvesting can be noted with the presence of higher vegetation density in unharvested areas in comparison to areas where thinning has occurred.

[INSERT FIGURE 1]

DATA

LiDAR Observations

An Optech ALTM 1225 LiDAR instrument was flown over the study site in August 24 of 2000. Mounted on a Piper Navajo aircraft, the instrument was flown at a speed of 60 m/s and at an altitude of 750 m above ground with a pulse repetition rate of 20 kHz. The scanning frequency was 15 Hz with a scan range of $\pm 15^{o}$ over a 400 m swath distance resulting in a footprint diameter of 15 cm. Elevation return measurements were calibrated using ground control points established with a survey-grade GPS

instrument across the study site. A 25% overlap of flight lines was obtained during the data acquisition in order to increase the density of LiDAR returns. REALM proprietary classification software (Optech Inc., 2000), designed to isolate LiDAR vegetation and ground return pulses, allowed for four discrete datasets of vegetation-first, vegetation-last, ground-first and ground-last returns to be classified. Within the one hectare study site, a total of 8662 laser pulse returns were obtained.

Six attributes were associated with each LiDAR return in the classified datasets: 1) a UTM Easting location, 2) a UTM Northing location, 3) the elevation of the return, 4) a unique flight line number corresponding to the flight pass being made, 5) the scan angle at which the LiDAR return was acquired, and 6) an intensity or amplitude for each detected return. Within this study, the first four attributes were used to evaluate ground and vegetation height.

Ground Observations

Tree Inventory

Due to previous intensive ground surveys conducted by the Canadian Forest Service – Great Lakes Forestry Centre, several stem-level datasets were made available for the one hectare shelterwood site. Within the study site, all 733 tree locations were referenced to benchmarks established over a 20 m grid using an electronic Sokkia DT6 theodolite. Tree locations were then geo-referenced to the UTM projection by establishing coordinate locations for the four corners of the study site using a survey-grade GPS receiver. Species identification and DBH were surveyed for all trees in the summer of July 1999. A second measurement of DBH was taken in November 1999 to confirm DBH values; maximum differences between measures were –1.2 cm and +1.7 cm.

Tree height and crown radius measurements were obtained using a vertex hypsometer for all trees identified as contributing to the upper-canopy. Where stems angled away from nadir, the offset angle

from nadir was measured. Two separate crown radius measurements were taken for all upper-canopy trees: (*i*) the distance to crown edge in the four cardinal directions at the crown base, and (*ii*) the distance to crown edge at the height of maximum crown radius. Using the crown radius measurements, crown ellipses were constructed as vector features within ArcInfo (Version 7.1.2, ArcEdit module) using coordinate geometry (COGO) functions. The upper-canopy of the study site is primarily dominated by mature trees with an average height of 18.73 m; 37% of these trees are below the average tree height. Visual description of upper-canopy vegetation cover can be obtained from the crown ellipses (**Figure 2**).

[INSERT FIGURE 2]

Optical Measurements of Radiation

The interaction of light within a forest canopy can be evaluated by measuring the amount of transmitted radiation. When solar radiation is transmitted through a canopy, the majority of incident short-wave radiation (> 700 nm) is absorbed by leaves while the remaining portions of radiation are transmitted or reflected within the canopy (Gates, 1980; Canham, 1999). A larger portion of longer wavelength radiation (< 700 nm) penetrates through the leaf structure. Photosynthetically-active radiation (PAR, 400 – 700 nm) represents the portion of the light spectrum which is used during photosynthesis.

Two optical instruments were used to measure radiation within the study site: a TRAC instrument (Tracing Radiation and Architecture of Canopies; Chen and Cihlar, 1995), and a Decagon AccuPAR Sunfleck Ceptometer (Model PAR–80, Version 3.0). The TRAC instrument allows continuous PAR sampling at ~ 1 cm intervals along straight transects perpendicular to the solar azimuth. Using a walking speed of 0.33 m/s and a sampling rate of 32 Hz, a sample density of ± 100 readings/m can be achieved.

The Ceptometer is a straight probe designed with 80 photodiodes spaced 1 cm apart allowing PAR measurements to be taken at a specific spatial resolution.

A total of eleven 100 m transects were established across the study site. To obtain measurements perpendicular to the Sun, five transects were measured at an azimuth of 170^0 South between 10:00 am and 11:00 am. An additional six transects were measured at an azimuth of 80^0 East between 1:00 pm and 3:30 pm. All measurements using the TRAC instrument were made during cloudless skies between 8-13 July 2002.

The TRAC instrument is designed to sample below-canopy PAR in one specific direction along a transect perpendicular to the Sun. Given that PAR transmittance is subject to scattering within a forest canopy (Canham, 1999), a bias may result from sampling PAR in a single direction. At each 10 m interval along each 100 m transect, PAR measurements were taken with the Ceptometer in the four cardinal directions (North, South, East and West). The 80 m probe was segmented into four sections allowing four sets of measurements to be taken at a spatial resolution of 20 cm. Due to the consistency of PAR observations from the Ceptometer and TRAC instruments, it was determined that the TRAC instrument accounted for multi-directional sources of transmitted radiation within the forest canopy (**Figure 3**).

Light transmittance was calculated for individual below-canopy PAR observations along each 100 m transect using the following equation:

$$LT = \frac{P_{below}}{P_{above}} \times 100 \qquad \text{(Eq. 1)}$$

where LT is the percentage of light transmittance below the canopy, P_{below} is a PAR measurement made below the canopy using the TRAC instrument, and P_{above} is a PAR measurement made in an open area within 100 m of the study site using a Li-Cor Point Quantum sensor (LI-190SA, LICOR, Lincoln, Neb.). The P_{above} sensor was positioned 3 m above the ground and attached to a datalogger (LI-1400, LICOR, Lincoln, Neb.) measuring incoming PAR at 15 second intervals.

[INSERT FIGURE 3]

Predicting Light Transmittance and Foliage Distribution

Spatial Variation and Geostatistics

A variety of techniques can be used to interpolate geo-spatial data (Bailey and Gatrell, 1998; Burrough and McDonnell, 1998). However, few techniques are based on an underlying model fitted to the spatial data. Geostatistics permits the modelling of spatial pattern by taking into account the spatial covariance during the interpolation process. Although other traditional point interpolation techniques such as inverse distance weighting can, in limited circumstances, provide predictions that are as accurate and less computationally intensive than kriging (Webster and Oliver, 1988; Isaaks and Srivastava, 1989), kriging can provide other benefits. It is known as a Best Linear Unbiased Predictor (BLUP); 'linear' in that predictions are weighted as a linear combination of the available data, and 'unbiased' with respect to the reduction of the mean residual error towards zero (Isaaks and Srivastava, 1989). Where traditional interpolation techniques use only distance-weighting independent of the data itself, kriging uses weights obtained by modelling the spatial dependence of the available data. Furthermore, residual and kriging variance surfaces provide information on the accuracy for the interpolated surfaces.

Spatial dependence is modelled for use in the kriging process using a semi-variogram. For continuous variables, such as elevation, the experimental semi-variance is defined as half the average

263 squared difference between values separated by a given lag **h**, where **h** is a vector in both distance and
264 direction (Eq. 2). Thus, the experimental semi-variogram $\gamma_v(\mathbf{h})$ may be obtained from α=1,2,…,$P(\mathbf{h})$ pairs
265 of observations $\{z_v(\mathbf{x}_a), z_v(\mathbf{x}_a+\mathbf{h})\}$ defined on a support *v* at locations $\{\mathbf{x}, \mathbf{x}+\mathbf{h}\}$ separated by a fixed lag **h**:
266
267
$$g_v(\mathbf{h})=\frac{1}{2P(\mathbf{h})}\sum_{a=1}^{P(\mathbf{h})}[z_v(\mathbf{x}_a)-z_v(\mathbf{x}_a+\mathbf{h})]^2 \quad \text{(Eq. 2)}$$
268
269
270 The spatial dependence between point locations is characterized by estimating three parameters of the
271 semi-variogram model: (*i*) the range *a*, (*ii*) the sill variance c_1, and (*iii*) the nugget variance, c_0. These
272 parameters are applied to the final kriging function to allow the modelling of spatial dependence in the
273 interpolated surface. The range provides a measure of the spatial arrangement of points based on their
274 distance and direction vector of separation. The sill variance provides a measure of spatial dependence.
275 The nugget variance provides a measure of spatially not autocorrelated noise within the dataset. It is
276 generally expected, based on Matheron's (1965) theory of regionalization, that as distance increases
277 features will become less related while features separated by shorter distances remain more closely
278 related.
279
280 *Minimum/Maximum Bias Removal*

281 A bias is known to occur in the leading-edge pulse returns for discrete-return LiDAR. Where
282 clumping of vegetation occurs at the top of the canopy, returns will provide a robust prediction of
283 vegetation height. However, where vegetation is more pervious with the presence of small gaps, the
284 leading-edge return will underpredict maximum vegetation height (Harding, 2002). Recent studies
285 support the use of interactive and low-pass filtering on the complete point cloud (Lim *et al.*, 2001) or
286 discrete-returns (Hyyppa *et al.*, 2001) to isolate maximum vegetation height within a specified distance of
287 each return.

A local filter was applied to isolate the two structural characteristics of interest in this study: canopy gaps and maximum vegetation height. Filtering was first applied to the leading-edge return pulses to isolate maximum vegetation height by assigning to each pulse return the maximum height within a given radius. Using a similar method, canopy gaps were discretized by assigning each LiDAR vegetation height return the minimum value within a given radius of each return. A range of filter radius values (0.25 m, 1.0 m, 2.5 m) was used to evaluate the effects of filtering on predictions of maximum height and canopy gaps. If the leading-edge bias is removed effectively, greater correspondence should be evident between ground observations of tree height and the percentage of transmitted light.

Trend Removal

One of the underlying assumptions of geostatistics is that all observations can be modelled as realizations of a stationary process (Isaaks and Srivistava, 1989). To make a prediction of the semi-variance between values at locations across a given area, it must be assumed that the behaviour of the process will be similar across space. An intrinsic stationary dataset must meet the requirement of having a constant mean and variance changing only as a function of distance. Anisotropy exists where either the amount or scale of variation changes with direction (Isaaks and Sravistava, 1989). A non-stationary, anisotropic surface can sometimes be made stationary by removing a global trend.

At each location *u* at which interpolation is required, Gooverts (1997) suggests first removing any global trend $\hat{m}(u)$ and then interpolating the residual values $\hat{r}(u)$ using kriging and the respective semi-variogram of the residuals. The final predicted surface is obtained by adding back the global trend $\hat{m}(u)$ to the interpolated residuals. If, as in our case, elevation observations are made on a linearly sloping surface, a linear trend is sufficient (Gooverts, 1997).

$$\hat{r}(u) = z(u) - \hat{m}(u) \qquad \text{(Eq. 3)}$$

Following the removal of a first-order trend from the ground-last LiDAR returns (**Figure 4a**), the first-order residuals were interpolated using ordinary kriging (**Figure 4b**). The first-order trend surface was then added back to the interpolated residuals to produce a final ground DEM (**Figure 4c**). The performance assessment of the prediction was carried out using stratified (or M-fold) cross-validation (Ripley, 1996). Each location *u* in the dataset is repredicted using all the data except for M randomly selected point. Repeating this process several (maximum $\binom{N}{M}$) times allows the characterization of prediction uncertainty by collecting the distribution of errors. We found a high level of correlation (R^2 = 0.96) between observed and cross-validated predictions of ground elevation supporting that an accurate ground elevation had been achieved (**Figure 5**). Further analysis suggests that this unbiased performance assessment provides a robust measure of the quality of the predictor as M varies between 20% and 80% (Lim *et al.*, unpublished).

[INSERT FIGURE 4]

[INSERT FIGURE 5]

Indicator Semi-variograms

The height of each LiDAR vegetation-first return above the ground surface was determined by subtracting each vegetation-first return from the interpolated ground surface. A cross-section of this LiDAR-derived vegetation height dataset ($V_{ht,}$ the height of LiDAR vegetation returns above ground elevation) can be viewed in **Figure 6a**.

Due to the pervious characteristics of the forest canopy surface and the footprint size and density of small-footprint discrete-return LiDAR, two vegetation returns can occur in close spatial proximity and provide an extreme range in vegetation height measurements. The result is a bimodal distribution of vegetation height across the study area which is a product of the intensity of small-footprint, discrete-

return LiDAR sampling and the vegetation structure. Interpolating the V_{ht} distribution directly using ordinary kriging will not provide an accurate prediction as such algorithms rely on assumptions of normality (Gooverts, 1997). To account for the bimodal characteristics in the V_{ht} distribution, indicator kriging was performed. Indicator kriging allows the evaluation of the V_{ht} distribution over a series of selected thresholds (Isaaks and Srivistava, 1989; Gooverts, 1997). The available continuous data $z(\mathbf{x}_a)$ may be transformed into an indicator variable $i_v(\mathbf{x}_a; z_k)$ defined as

$$i(\mathbf{x}_a; z_k) = \begin{cases} 1 & \text{if } z(\mathbf{x}_a) \le z_k \\ 0 & \text{otherwise} \end{cases} \quad \text{(Eq. 4)}$$

for a given threshold (or cut-off) z_k. Then it is possible to obtain experimental indicator functions from these indicator data. The experimental indicator semi-variogram $\gamma_{vI}(\mathbf{h}; z_k)$ (where, $\mathbf{h}$; z_k is read as lag $\mathbf{h}$ given the threshold z_k) may be obtained from indicator data $i_v(\mathbf{x}_a; z_k)$ as:

$$g_{vI}(\mathbf{h}; z_k) = \frac{1}{2P(\mathbf{h})} \sum_{a=1}^{P(\mathbf{h})} [i_v(\mathbf{x}_a; z_k) - i_v(\mathbf{x}_a + \mathbf{h}; z_k)]^2 \quad \text{(Eq. 5)}$$

Generally, k thresholds will be defined resulting in k indicator semi-variograms. Often, the nine percentiles of the cumulative distribution function (CDF) are chosen as the indicator thresholds resulting in nine indicator semi-variograms. However, the choice of number of cut-offs clearly depends on the number of available data amongst other considerations. This non-parametric approach has been applied previously to characterize the probability of soil contamination (Meirvenne and Goovaerts, 2001) and water temperature (Fabri, 2001) where an accurate interpolation of non-normally distributed environmental attributes was required.

363 Since the experimental semi-variogram provides only discrete values of the semivariance g at a set of
364 discrete lags $\mathbf{h}_1$, $\mathbf{h}_2$,... it is necessary to fit a continuous mathematical model for statistical inference. Not
365 any mathematical function will do. Specifically, the semi-variogram $g(\mathbf{h})$ of the random function (RF)
366 must be conditional negative semi definite (CNSD). Semi-variogram models with the CNSD property are
367 called permissable or 'authorized'. Practitioners usually choose from the set of known authorized
368 functions. Four of the most common functions in general use are the nugget effect, spherical, exponential
369 and Gaussian models. Each can be described according to its characteristic shape. All four models are
370 bounded (transitive) because they include a maximum value of semi-variance known as the sill. For the
371 spherical model the sill is reached within a finite lag known as the range a. For the exponential and
372 Gaussian models the sill is approached asymptotically. Since the exponential and Gaussian models never
373 reach the sill, it is necessary to define a *practical range* $a'=3r$ in place of the definite range. The nugget
374 effect model is a 'flat' model representing a constant positive semi-variance at all lags; thus, it too has a
375 sill. Further, whereas the other models intercept the ordinate at the origin, the nugget effect model
376 represents a discontinuity at the origin.
377
378 There are many different ways to fit models to experimental semi-variograms, including completely
379 automatic fitting and fitting by eye. The best solution is often a compromise between these two (semi-
380 automatic fitting) where the user chooses a type of semi-variogram model (based partly on the sample
381 function and partly on *a priori* knowledge), decides whether an anisotropic model is required, and then
382 obtains a fit for these choices using weighted least sum of squares (*WWS*) approximation given by:
383
384
$$WSS = \sum_{k=1}^{K} w(\mathbf{h}_k) \cdot [\hat{g}(\mathbf{h}_k) - g(\mathbf{h}_k)]^2 \qquad \text{(Eq. 6)}$$
385
386

The V_{ht} dataset was reclassified into nine indicator variables using the nine percentiles $z_{k1\text{-}9}$ of the distribution. Each indicator threshold z_k essentially represents a different height within the foliage (**Figure 6a**). Indicator semi-variograms were created for each binary variable allowing the spatial structure at each height threshold to be modelled (**Figure 6b**). The best least-squared fit in each case was provided by the spherical model, which in theory, is an appropriate model for deciduous canopy structure due to the size, shape and density of tree crowns and intercrown spaces (Treitz, 2001). Smaller values of semi-variance occurred at the upper and lower indicator threshold heights $z_{k1\text{-}3,8\text{-}9}$. As expected, the largest values of semi-variance occurred at intermediate threshold heights $z_{k4\text{-}7}$. The ranges at upper indicator thresholds $z_{k3\text{-}9}$ maintained a similar value of ~13 m with the exception of lower thresholds $z_{k1\text{-}2}$, which varied between18 – 20 m.

[INSERT FIGURE 6]

Indicator Probability Maps

The public domain geostatistics software package GSLIB (Deutsch and Journel, 1998) was used to perform indicator kriging. Using the series of binary indicator variables classified from V_{ht} and their respective semi-variograms, a series of indicator probability maps were created. At each indicator threshold z_k, a conditional probability was predicted at all unsampled locations by applying ordinary kriging (Bierkens and Burrough, 1993). Probability values for each threshold surface represent the likelihood of exceeding the threshold z_k within each cell. As a result, each threshold surface provides a continuous measure of vegetation probability (*i.e.*, the probability of a LiDAR pulse being returned from foliage at the associated indicator threshold height z_k, hereafter referred to as PVz_k) characterizing the probability of being vegetated or non-vegetated (open gap space) at that given threshold. A final cumulative PVz_k surface can then be constructed by obtaining a total of all $z_{k1\text{-}9}$ threshold surfaces on a per cell basis. In theory, this final cumulative PVz_k surface will provide a description of light

transmittance probability by taking into account the probability of gap and vegetation structure along both the vertical and horizontal profiles of the canopy.

Comparing Ground and LiDAR Observations

The accuracy of the indicator kriging predictions can be assessed using ground observations of tree height and light transmittance. A non-linear relationship is expected between light transmittance and vegetation height since the distribution of light transmittance is typically non-uniform at different heights within a forest canopy environment (Parker, 1995). Observed light transmittance measurements and predicted PVz_k surfaces were then aggregated over a range of spatial resolutions (0.25 m, 1.0 m and 2.5 m) and their correlations calculated. PVz_k surfaces were aggregated spatially by performing indicator kriging at coarser spatial resolutions. Ground observations of light transmittance were aggregated to the same spatial resolutions by spatial filtering. It is expected that the probability of light transmittance will vary as a function of vegetation density. Specifically, the probability of light transmittance is expected to be high where canopy gaps are present and low where vegetation density is high.

A similar technique was used to compare ground observations of tree height to each filtered and non-filtered PVz_k surface. Each PVz_k surface was evaluated for the correspondence between the location of observed tree heights exceeding each indicator threshold z_k and the PVz_k value predicted for each tree location.

It was found after initial attempts to relate predictions of vegetation probability from LiDAR to ground-based measures of tree height that tree crowns and the maximum height of each tree were not necessarily located directly above each stem location. To account for the offset of maximum vegetation height from the stem location, the maximum PVz_k value was obtained within a 2.5 m radius of each stem.

RESULTS AND DISCUSSION

Filtering to Remove Bias in LiDAR Returns

Minimum and maximum filtering applied to the V_{ht} dataset did not result in an observable change in the relationship between ground observations of light transmittance and tree height. It is expected that the leading-edge ranging bias was removed during the aggregation of the LiDAR data to spatial resolutions greater than the nominal footprint diameter.

A Three-Dimensional Representation of Foliage Distribution

Figure 7 presents a three-dimensional representation of the indicator probability surfaces based on the nine percentiles of the LiDAR V_{ht} dataset. Variation in the probability of vegetation height can be noted over the nine indicator threshold surfaces. At smaller threshold heights $z_{k1\text{-}2}$, the boundaries of lower canopy gaps are apparent which then increase in size when evaluated at larger thresholds $z_{k3\text{-}9}$. Detailed canopy characteristics are captured using a fine spatial resolution of 0.25 m.

Modelled semi-variance parameters from the V_{ht} dataset were found to provide a description of the vertical and horizontal forest canopy with semi-variance changing as a function of the vegetation structure at the nine threshold heights. Lower semi-variance values occurred at the lower and upper threshold heights $z_{k1\text{-}2,8\text{-}9}$ within the canopy corresponding with the presence of smaller variability in foliage distribution around the top of the canopy and close to the ground (i.e., understory), respectively. Semi-variance increased at the middle thresholds of the canopy $z_{k3\text{-}7}$ where the canopy is structurally more complex.

The range of the semi-variograms remained fairly consistent over the series of indicator thresholds with the exception of lower threshold heights $z_{k1\text{-}2}$. It is apparent from the probability surfaces for each indicator threshold that open areas in the forest canopy are separated by larger distances at smaller

thresholds $z_{k1\text{-}2}$. At larger thresholds $z_{k3\text{-}9,}$ range values vary less between thresholds indicating a more consistent spatial pattern of features in the mid-canopy and the over-story. This lack of variation in the range may be attributed to the study site being dominated by a single-species, sugar maple forest canopy.

The above results demonstrate typical characteristics of a deciduous forest canopy where vegetation complexity is lower in the sub-canopy with increasing structural complexity in the mid-canopy (Oliver, 1990). A recent study by Parker *et al*. (2001) found similar results using large-footprint, full-waveform LiDAR where the spatial variation of vegetation structure was found to change as a function of height within the forest canopy.

[INSERT FIGURE 7]

Ground Measured PAR and Gap Probability

The relationships between observed light transmittance values and the cumulative PVz_k surface were evaluated for three spatial resolutions. Ground measurements of PAR provided greater correspondence to the LiDAR-based prediction of cumulative PVz_k as the data were spatially aggregated from a spatial resolution of 0.25 m to 2.5 m (**Figure 8**). We found a negative log-linear relationship between percentage of light transmittance and cumulative PVz_k. Since the optimal spatial resolution for analysis is related, among other things, to the characteristics of the objects being analyzed (Jupp *et al*., 1988; Atkinson and Curran, 1995) and the locational accuracy of ground observations, the results of this analysis suggest that vegetation structure and light transmittance should be evaluated at spatial resolutions of 2.5 m.

[INSERT FIGURE 8]

485 *Ground Measured Tree Height and Foliage Distribution*

486 The PVz_k surfaces were further assessed by comparing observed tree heights exceeding each indicator
487 threshold. Theoretically, all observed tree heights greater than each indicator threshold should correspond
488 with areas of high vegetation probability at the same threshold height. PVz_k surfaces at lower threshold
489 heights were found to correspond with observed tree heights exceeding the respective threshold. At the
490 4th height threshold (**Figure 9a**) it was apparent that all trees with heights greater than 13.83 m correspond
491 well with areas of high vegetation probability. This high level of correspondence between observed tree
492 heights and predicted vegetation probability is maintained up to the 7th threshold height of 18.73 m.
493 Above the 7th threshold height (**Figure 9b**), the correspondence between observed and expected
494 vegetation height decreases to less than 70%.
495
496 Several sources of error may be associated with the low correspondence above the 7th threshold
497 height. First, a random elevation error of 30 to 50 cm occurred with the Timing Interval Measurement
498 (TIM) unit when the data were acquired. The TIM unit allows the time interval between the laser pulse
499 leaving the aircraft and the return of the reflected pulse back to the sensor to be measured precisely. This
500 error applied only to the LiDAR last-return datasets. Secondly, measuring tree height from the ground
501 using a vertex hypsometer becomes more difficult as tree height increases due to overlapping vegetation
502 and the angle at which measurements are taken. This may add uncertainty to the ground observations and
503 result in the lack of correspondence with PVz_k surfaces for the upper threshold heights $z_{k7\text{-}9}$.
504
505 [INSERT FIGURE 9]
506
507 **CONCLUSIONS**

508 This study suggests that interpolations of the vegetation-return from small-footprint, discrete-return
509 LiDAR can provide fine spatial resolution information on the probability of vegetation within deciduous

canopy environments. Through the use of indicator kriging, horizontal slices of vegetation probability are obtained over a series of canopy threshold heights. The high correlation between these vegetation probability surfaces and observed measurements of light transmittance suggest that light transmittance can also be predicted based on gap and non-gap space. The correlation between observed and LiDAR-based predictions of light transmittance increased as the data were spatially aggregated to a spatial resolution of 2.5 m. Evaluating semi-variance at specific threshold heights within the forest canopy provided a description of the horizontal pattern of vegetation structure.

While this work has served as a feasibility assessment to evaluate methods for mapping the vegetation-return from small-footprint, discrete-return LiDAR, several management and research incentives are offered. As a predictive tool, small-footprint LiDAR can be used to obtain information on the horizontal and vertical distribution of foliage and light transmittance within forest canopies.

Operating as a diagnostic tool, these indicator probability surfaces can be used to obtain detailed information about the distribution of light, structure, health and habitat in forests for management. Further, by evaluating semi-variogram model parameters over a series of threshold heights within the forest canopy additional information is obtained on the spatial characteristics of forest structure at each threshold. Recent studies suggest that evaluating the spatial variation in fine spatial resolution data over a range of spatial resolutions can provide information on forest health, such as chlorophyll content and other physiological conditions (Sampson *et al*., 2002).

Additional research may consider applying the methodology of this study over larger spatial extents and in areas with other and/or variable vegetation cover. Extending our findings to larger areas is challenging due to the requirement of stationarity and consideration of multiple species/multiple architecture effects.

Future research will also make use of fine spatial resolution light transmittance surfaces generated from LiDAR to explore light dynamics within forest canopies. The detailed information within the vegetation probability surfaces may allow vegetation clumping and the size and distribution of canopy gaps to be evaluated. Recent studies on light dynamics within forests have focused on the spatial location and size of gaps within forest canopies (Chen *et al.*, 1997, Canham *et al*., 1999). These studies have suggested that measures of vegetation clumping will provide greater accuracy in predictions of light transmittance within closed-forest environments. By characterizing the spatial distribution of vegetation clumping and indirect paths of light penetration through geometrical optical modelling, greater correspondence may be obtained between fine spatial resolution predictions of forest structure from LiDAR.

Advances in current small-footprint LiDAR instruments may also provide additional information for determining forest structure. Future small-footprint, discrete-return LiDAR instruments may provide full-waveform information for a small percentage of measured returns (Flood, 2002). While full-waveform information cannot feasibly be acquired for all small-footprint LiDAR returns due to data storage limitations, the detailed information from the complete waveform could be used to determine the accuracy of predictions of foliage structure. Recent research on interpreting full-waveform LiDAR (Lefsky *et al*., 1999a; Lefsky *et al*., 1999b; Harding *et al*., 2001; Parker *et al*., 2001) could be integrated with the density of small-footprint, discrete-return LiDAR measurements and provide greater accuracy in predictions of forest structural variables moving from individual-based observations to quasi-continuous fields.

558 ## ACKNOWLEDGEMENTS

559 This work was supported by Geomatics for Informed Decisions (GEOIDE RES#50) Network of
560 Centres of Excellence, the Centre for Research in Earth and Space Technologies (CRESTech) to F.
561 Csillag, and by the Royal Society (Exchange Grant) to P. Atkinson. We thank P. Belanger of LaserMap
562 Image Plus and M. Flood of Airborne 1 Inc. for assistance with LiDAR data acquisition. The assistance
563 of A. Groot (CFS-Sault Ste. Marie), who provided forest mensuration data and field equipment resources,
564 J. Chen (University of Toronto) and I. Creed (University of Western Ontario) who provided field
565 equipment and logistical support and M. Burchfield (University of Toronto) who assisted with collection
566 of the ground data, is gratefully acknowledged.

567

REFERENCES

Atkinson, P.M., Curran, P.J. (1995). "Defining an optimal size of support for remote sensing investigations." *IEEE Transactions on Geoscience and Remote Sensing*, Vol. 33, No. 3, pp. 768-776.

Bailey T.C. and Gatrell, A.C. (1995). *Interactive spatial data analysis.* Essex: Longman Group Ltd., 413p.

Burrough, P.A. and McDonnell, R.A. (1998). "*Principles of geographical information systems*", New York: Oxford University Press, 333p.

Canadian Council of Forest Ministers (CCFM). (1997). *Criteria and indicators for sustainable forest management in Canada:Technical Report*, Natural Resources Canada - Canadian Forest Service, Ottawa, 122p.

Canham, C.D., Coates, K.D., Bartemucci, P., and Quaglia, S. (1999). "Measurements and modeling of spatially explicit variation in light transmission through interior cedar-hemlock forests of British Columbia", *Canadian Journal of Forest Research*, Vol. 29, pp. 1775-1783.

Chen, J.M., and Cihlar, J. (1995). "Plant canopy gap-size analysis theory for improving optical measurements of leaf-area index", *Applied Optics*, Vol. 34, No. 27, pp. 6211-6222.

Chen, J.M. and Cihlar, J. (1996). "Retrieving leaf area index of boreal conifer forests using Landsat TM images", *Remote Sensing of Environment*, Vol. 55, pp. 153-162.

591 Chen, J.M., Rich, P.M., Gower, S.T., Norman, J.M., and Plummer, S. (1997). “Leaf area index of
592 boreal forests: theory, techniques and measurements”, *Journal of Geophysical Research*, Vol. 102, No.
593 24, pp. 429-443.
594
595 Chen, J.M., Lui, J., Cihlar, J., and Goulden, M.L. (1999). “Daily canopy photosynthesis model
596 through temporal and spatial scaling for remote sensing applications”, *Ecological Modelling*, Vol. 124,
597 pp. 99-119.
598
599 Decagon Devices Inc. (2001). *AccuPAR PAR/LAI Ceptometer Operator’s Manual*. Pullman, WA,
600 155p.
601 Deutsch, C.V., and Journel, A.G. (1998). *GSLIB: Geostatistical software library and user's guide*.
602 New York, Oxford University Press, 369p.
603
604 Fabri, P. (2001). “Probablistic assessment of temperature in the Euganean geothermal area”,
605 *Mathematical Geology*, Vol. 33, No. 6, pp. 745-760.
606
607 Flood, M. (2002). “From commercial data to commercial products: research priorities in the
608 commercial sector”, *International Workshop on Three-dimensional Analysis of Forest Structure and*
609 *Terrain using LiDAR technology*, Victoria, March 12-15, 2002.
610
611 Gates, D.M. (1980). *Biophysical plant ecology*. New York, Springer-Verlag, 609p.
612
613 Goodale, C.L., Apps, M.J., Birdsey, R.A., Field, C.B., Heath, L.S., Houghton, R.A., Jenkins, J.C.,
614 Kohlmaier, G.H., Kurz, W., Lui, S.R., Nabuurs, G.J., Nilsson, S., and Shvidenko, A.Z. (2002). “Forest
615 carbon sinks in the Northern Hemisphere”, *Ecological Modelling*, Vol. 12, No. 3, pp. 891-899.
616

617 Gooverts, P. (1997). *Geostatistics for natural resources evaluation*. New York, Oxford University
618 Press, 483p.
619
620 Harding, D.J., Lefsky, M.A., Parker, G.G., and Blair, J.B. (2001). "Laser altimeter canopy height
621 profiles: methods and validation for closed-canopy broadleaf forests", *Remote Sensing of Environment*,
622 Vol. 76, pp. 283-297.
623
624 Harding, D.J. (2002). "NASA airborne and space-based laser altimeters: from waveforms to
625 photons", *International Workshop on Three-dimensional Analysis of Forest Structure and Terrain using*
626 *LiDAR*, Victoria, March 12-15, 2002.
627
628 Hyyppa, J., Kelle, O., Lehikoinen, M., and Inkinen, M. (2001). "A segmentation-based method to
629 retrieve stem volume estimates from 3-D tree height models produced by laser scanners", *Transactions on*
630 *Geoscience and Remote Sensing*, Vol. 39, No. 5, pp. 969-975.
631
632 Intergovernmental Panel on Climate Change (IPCC). (2001). *Climate Change 2001 - The Scientific*
633 *Basis: contribution of working group I to the third assessment report of the IPCC*. Cambridge, Cambridge
634 University Press, 994p.
635
636 Isaaks, E.H., and Srivastava, R.M. (1989). *An introduction to applied geostatistics.* New York,
637 Oxford University Press, 561p.
638
639 Jupp, D.L.B., Strahler, A.H., and Woodcock, C.E. (1988). "Autocorrelation and regularization in
640 digital images I. Basic theory", *IEEE Transactions on Geoscience and Remote Sensing*, Vol. 26, No. 4,
641 pp. 463-473.
642

Lefsky, M.A., Harding, D., Cohen, W.B., Parker, G., and Shugart, H.H. (1999a). "Surface *LiDAR* remote sensing of basal area and biomass in deciduous forests of Eastern Maryland, USA", *Remote Sensing of Environment*, Vol. 67, pp. 83-98.

Lefsky, M.A., Cohen, W.B., Acker, S.A, Parker, G.G., Spies, T.A., and Harding, D. (1999b). "LiDAR remote sensing of the canopy structure and biophysical properties of Douglas-fir western hemlock forests", *Remote Sensing of Environment*, Vol. 70, pp. 339-361.

Lieffers, V.J., Messier, K.J., Stadt, K.J., Gendron, F., and Comeau, P.G. (1999). "Predicting and managing light in the understory of boreal forests", *Canadian Journal of Forest Research*, Vol. 29, pp. 796-811.

Lieth, H. and Whittaker, R.H. (1975). *Primary productivity of the biosphere*. New York, Springer-Verlag Inc, 339p.

Lim, K., Treitz, P., Groot, A., and St-Onge, B. (2001). "Estimation of individual tree heights using LiDAR remote sensing", *Proceedings of the Twenty-Third Annual Canadian Symposium on Remote Sensing*, Quebec, August 20-24, 2001.

Lim, K., Csillag, F., Todd, K., and Treitz, P. (unpublished). "Bootstrap cross-validation of fine resolution elevation data derived from LiDAR", International Geoscience and Remote Sensing Symposium, Toronto, June 24-28, 2002.

Lui, J., Chen, J.M., Cihlar, J., and Chen, W. (2002). "Net primary productivity mapped for Canada at 1 km resolution", *Global Ecology and Biogeography*, Vol. 11, pp. 115-129.

669 Matheron, G. (1965). Les Variables Regionalisees et Leur Estimation. Masson, Paris.

670

671 Means, J.E., Acker, S.A., Harding, D.J., Blair, J.B., Lefsky, M.A., Cohen, W.B., Harmon, M.E., and
672 McKee, W.A. (1999). "Use of large-footprint scanning airborne *LiDAR* to estimate forest stand
673 characteristics in the western cascades of Oregon", *Remote Sensing of Environment*, Vol. 67, pp. 298-308.

674

675 Meirvenne, M.V., and Goovaerts, P. (2001). "Evaluating the probability of exceeding a site-specific
676 soil cadmium contamination threshold", *Geoderma*, Vol. 102, pp. 75-100.

677

678 Morrison, I.K., Cameron, D.A., Foster, N.W., and Groot, A. (1999). "Forest research at the Turkey
679 Lakes Watershed", *The Forestry Chronicle*, Vol. 75, No. 3, pp. 395-399.

680

681 Oliver, C.D. (1990). *Forest stand dynamics*. New York, McGraw-Hill Inc, 467p.

682

683 Parker, G. (1995). Structure and microclimate of forest canopies, *In:* Lowman, M. and Nadkarni, N.
684 (eds). *Forest Canopies: A review of research on a biological frontier*. San Diego: Academic Press.

685

686 Parker, G., Lefsky, M.A., and Harding, D.J. (2001). "Light transmittance in forest canopies
687 determined using airborne laser altimetry and in-canopy quantum measurements", *Remote Sensing of*
688 *Environment*, Vol. 76, pp. 298-309.

689

690 Ripley, B.D. (1996). *Pattern recognition and neural networks.* New York, Cambridge University
691 Press, 403p.

692

Sampson, P.H., Treitz, P.M., and Mohammed, G.H. (2001). "Remote sensing of forest condition in tolerant hardwoods: an examination of spatial scale, structure and function", *Canadian Journal of Remote Sensing*, Vol. 27, No. 3, pp. 232-246.

Treitz, P. and Howarth, P. (1996). *Remote sensing for forest ecosystem characterization: a review.* Nat. Resource Canada, Canadian Forest Service, Sault Ste. Marie, NODA/NFP Tech. Rep. TR-12, 51p.

Treitz, P. (2001). "Variogram analysis of high spatial resolution remote sensing data: An examination of boreal forest ecosystems", *International Journal of Remote Sensing*, Vol. 22, No. 18, pp. 3895-3900.

Waring, R.H. and Running, S.W. (1998). *Forest Ecosystems: Analysis at multiple scales.* New York, Academic Press Inc, 370p.

FIGURE 1.

The location of the study site with respect to the harvest blocks for the Harvest Impact Study within the Turkey Lakes Watershed. The inset shows the location of the study area within Ontario, Canada.

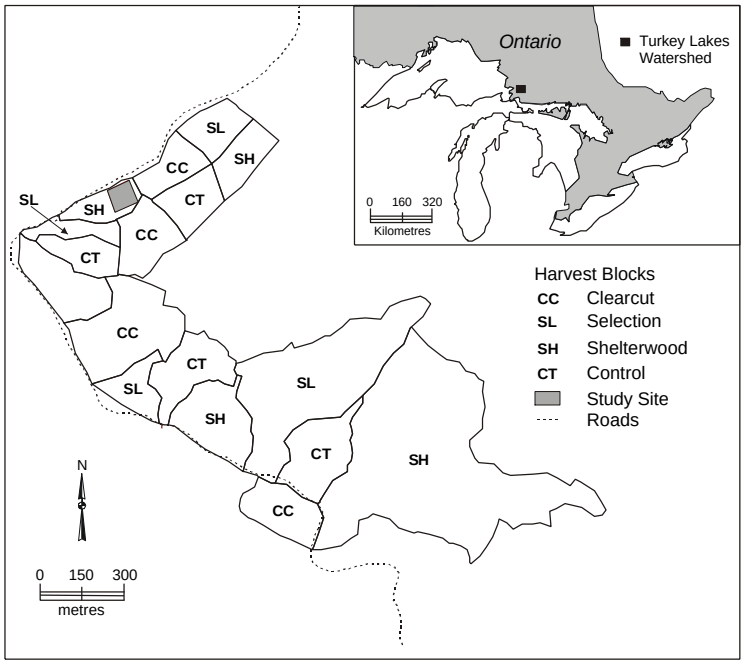

FIGURE 2.

Tree heights and crown ellipses for all upper-canopy trees (n = 186) within the one hectare study site. All trees and crown edges have been georeferenced to a local coordinate system using surveying and GPS measurements.

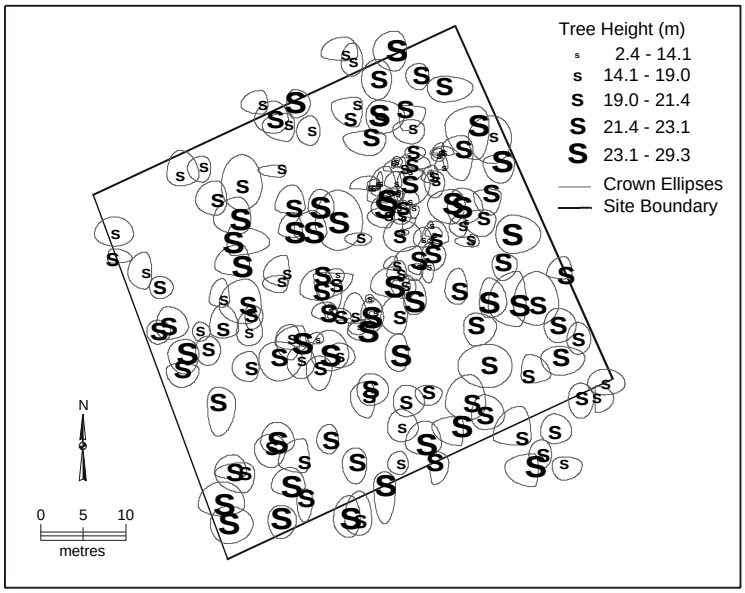

718 **FIGURE 3.**

719 PAR measurements acquired at ~1 cm intervals along a 100 m transect using the TRAC instrument.
720 Boxes represent 10 m observations of PAR from the AccuPAR Ceptometer measured in the four cardinal
721 directions (North, South, East, West).

722

723

724

725

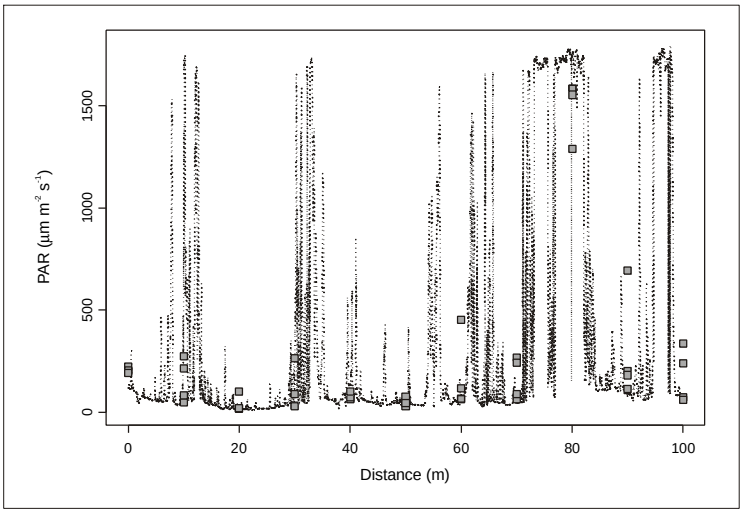

725 **FIGURE 4.**

726 Interpolations used to generate the final ground surface using the LiDAR ground-last returns where (a) is
727 the first-order polynomial trend, (b) is the ordinary kriging interpolation of the first-order residuals, (c) is
728 the final ground surface, and (d) is the kriging variance of the first-order residuals.

729

730

731

732

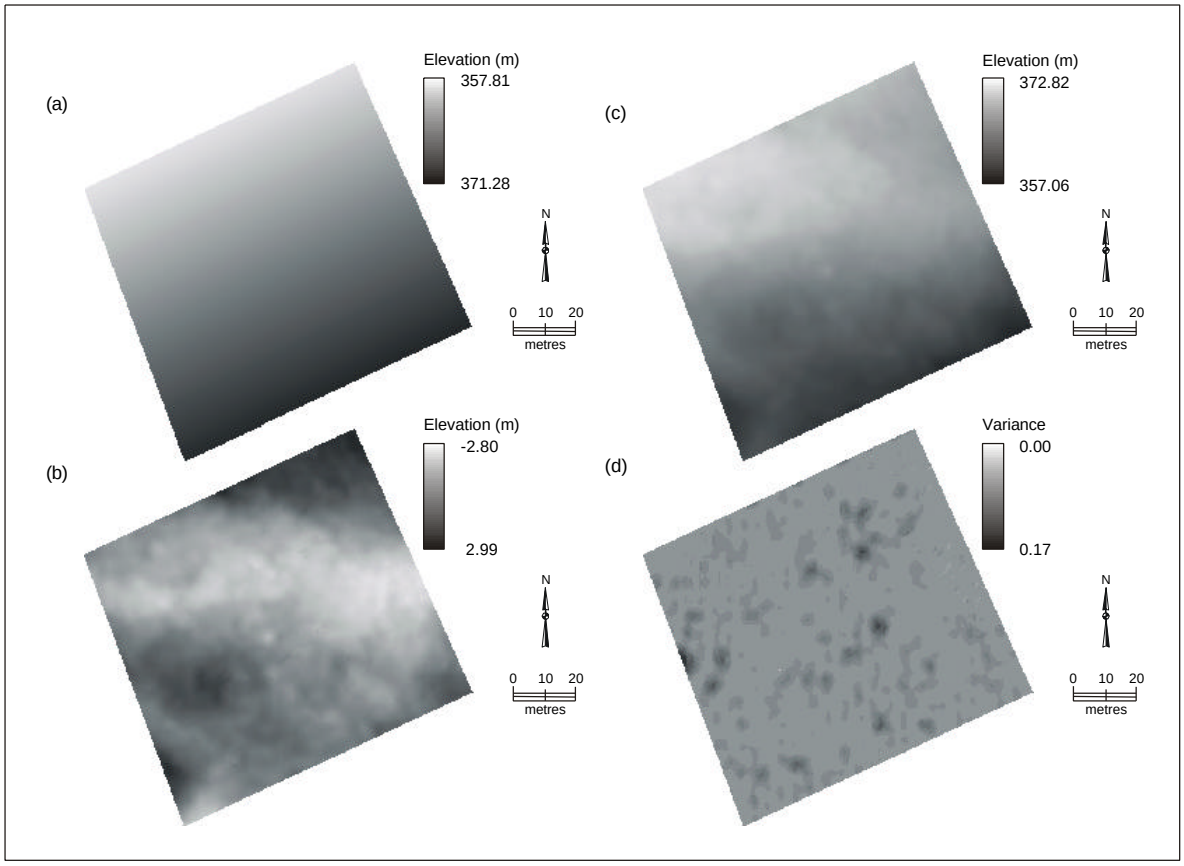

732 **FIGURE 5.**

733 A cross-validation plot between LiDAR ground-last return elevations and predicted ground elevations
734 using ordinary kriging. The dashed line represents a 1:1 relationship (0 intercept, slope 1). The solid line
735 represents a least-squared fit between observed and predicted elevations.

736

737

738

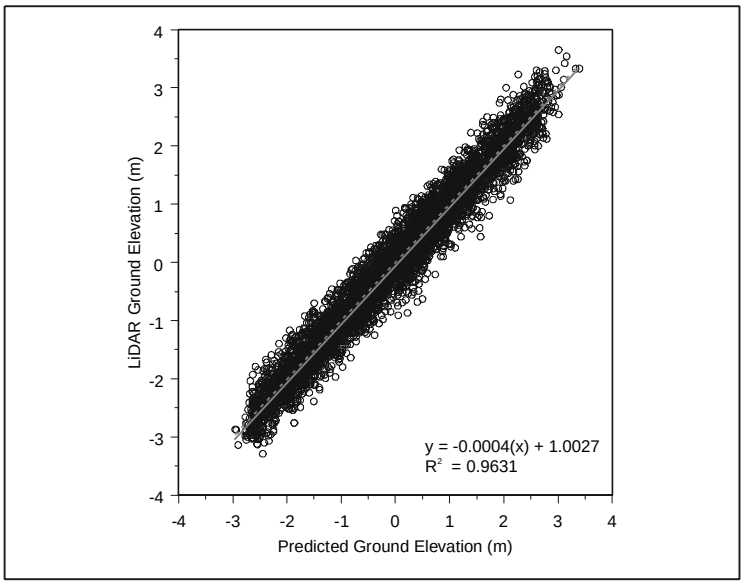

738 **FIGURE 6.**

739 Plots of (a) LiDAR vegetation-returns in an easterly direction across the study site with indicator
740 thresholds marked at the nine percentiles of the distribution, and (b) semi-variograms modelled for the
741 binary datasets created for each indicator height threshold.

742

743

744

745

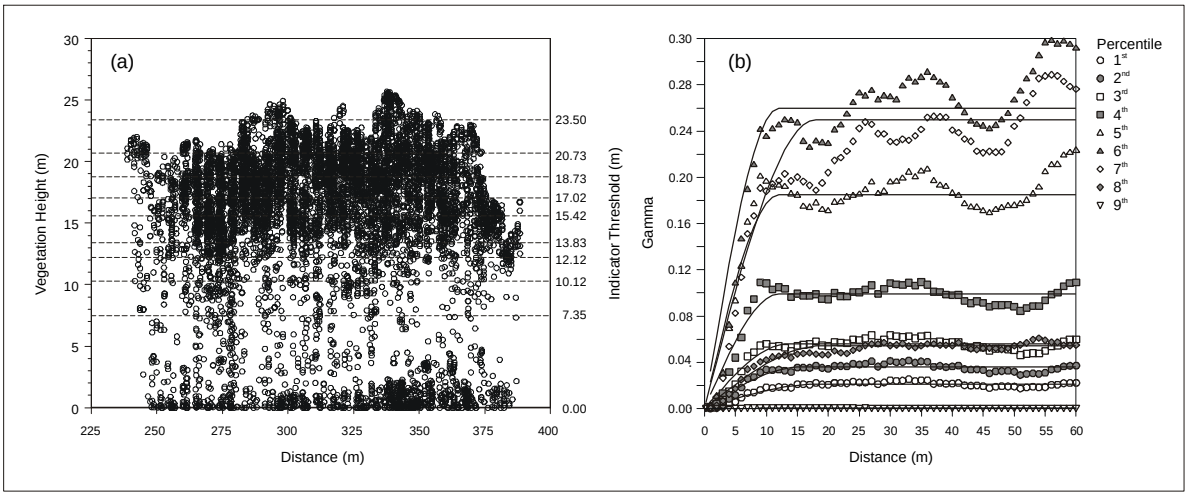

FIGURE 7.

Indicator probability surfaces for nine percentiles of vegetation height within the study area. Probability values for each threshold surface represent the probability of exceeding the indicator threshold height. 0.00 (green) being low probability and 1.00 (beige) being high probability. The plot depicts semi-variance and the cumulative distribution function corresponding to each indicator height threshold.

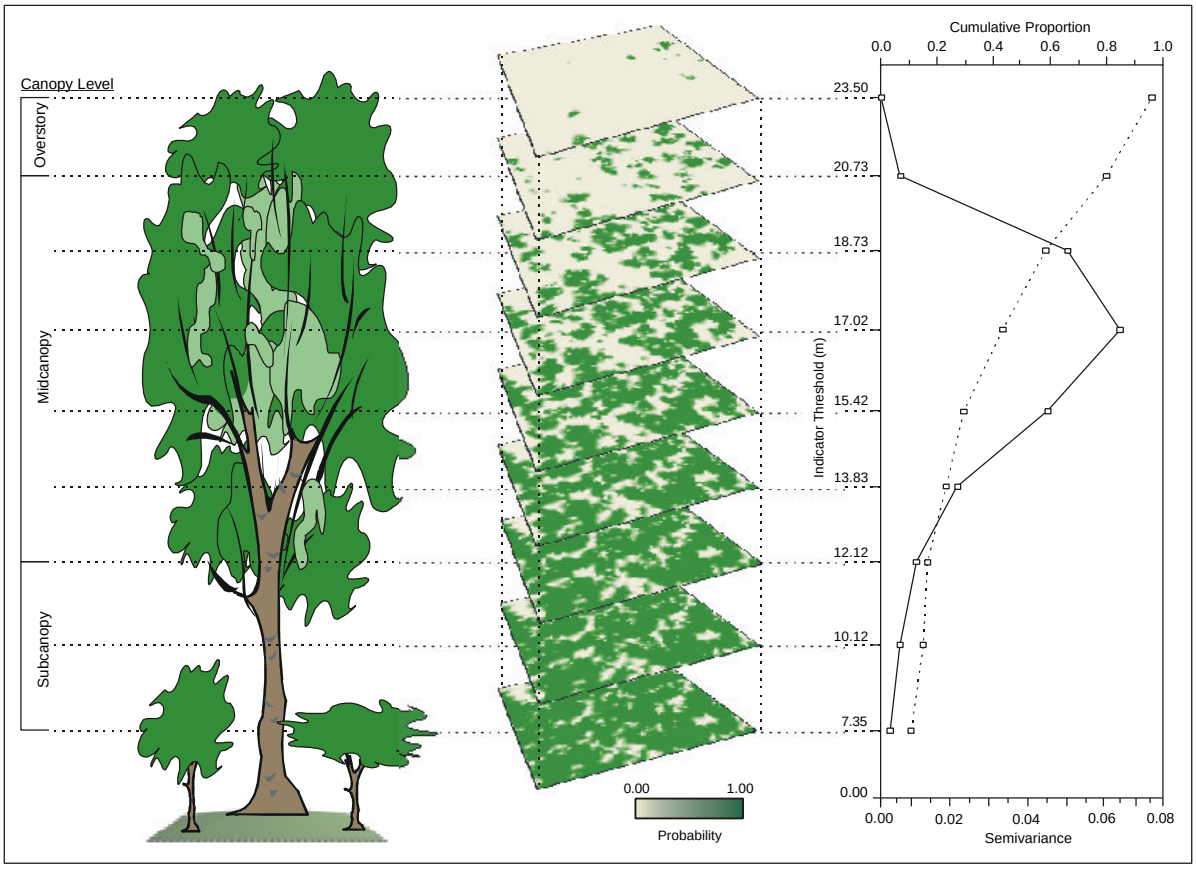

752 **FIGURE 8.**

753 Relationships between observed light transmittance and indicator vegetation probability for the first
754 percentile surface and a cumulation of the nine percentile surfaces over three spatial resolutions: 0.25 m,
755 1.0 m and 2.5 m.

756

757

758

759

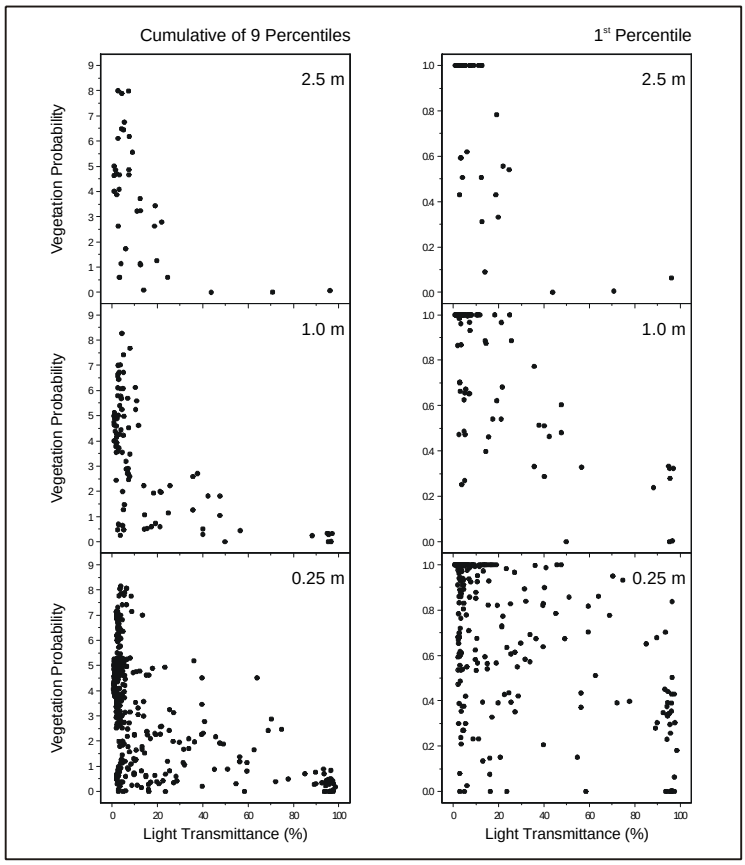

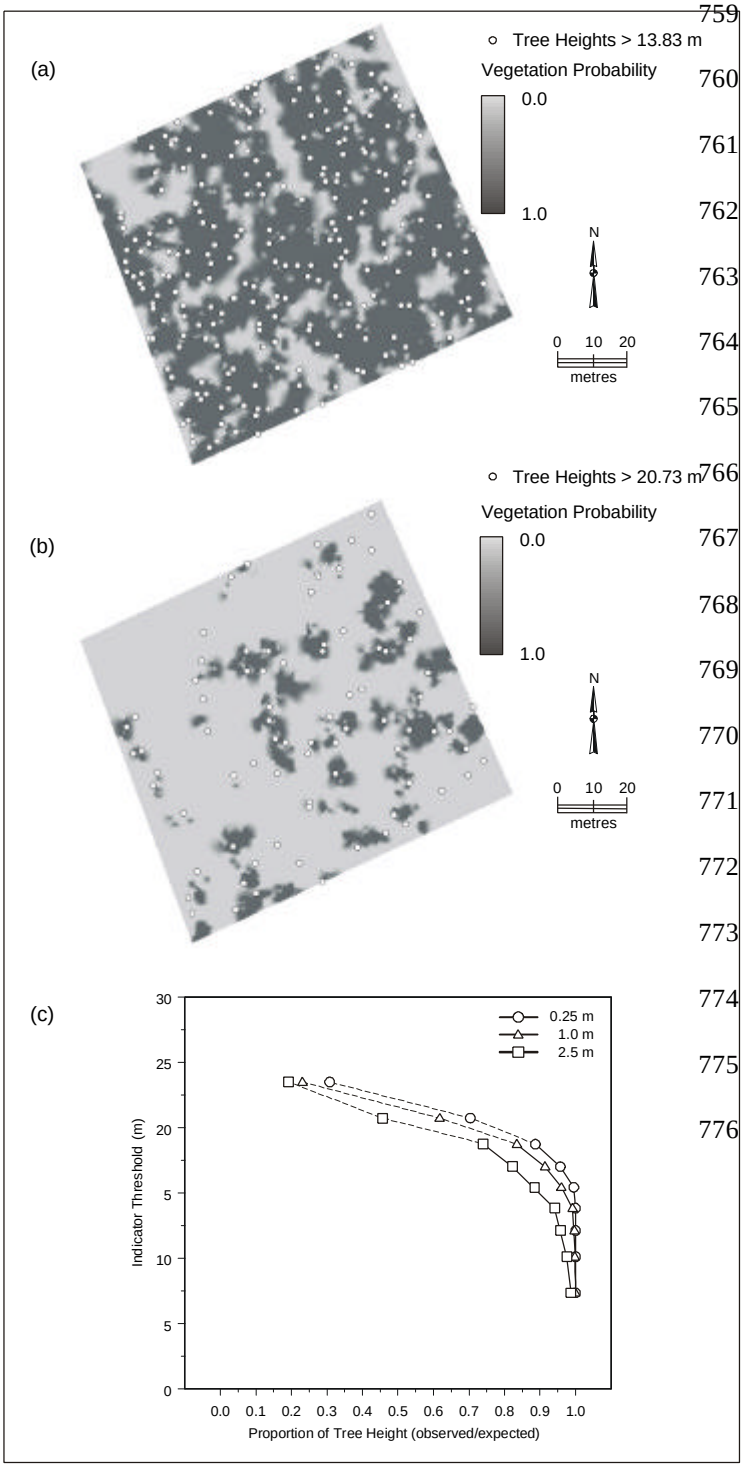

FIGURE 9.

Observed tree heights exceeding the indicator threshold in association to the indicator probability surface, where (a) illustrates the 4th indicator threshold of 13.83 m and (b) illustrates the 8th indicator threshold of 20.73 m. The plot (c) depicts the relationship between accurately predicted vegetation heights (observed vs. expected) for each indicator threshold over three spatial resolutions. Dashed lines after the 7th threshold value note where a marked decrease occurs in the proportion of accurately predicted vegetation heights.